



Lightweight Mechanical Metamaterials with Tunable Negative Thermal Expansion

Qiming Wang,^{1,*} Julie A. Jackson,² Qi Ge,^{3,4} Jonathan B. Hopkins,⁵ Christopher M. Spadaccini,² and Nicholas X. Fang^{3,†}

¹*Sonny Astani Department of Civil and Environmental Engineering,*

University of Southern California, Los Angeles, California 90089, USA

²*Lawrence Livermore National Laboratory, Livermore, California 94550, USA*

³*Department of Mechanical Engineering, Massachusetts Institute of Technology, Cambridge, Massachusetts 02139, USA*

⁴*Digital Manufacturing and Design Centre, Singapore University of Technology and Design, 487372, Singapore*

⁵*Department of Mechanical and Aerospace Engineering, University of California, Los Angeles, California 90095, USA*

(Received 4 May 2016; published 21 October 2016)

Ice floating on water is a great manifestation of negative thermal expansion (NTE) in nature. The limited examples of natural materials possessing NTE have stimulated research on engineered structures. Previous studies on NTE structures were mostly focused on theoretical design with limited experimental demonstration in two-dimensional planar geometries. In this work, aided with multimaterial projection microstereolithography, we experimentally fabricate lightweight multimaterial lattices that exhibit significant negative thermal expansion in three directions and over a temperature range of 170 degrees. Such NTE is induced by the structural interaction of material components with distinct thermal expansion coefficients. The NTE can be tuned over a large range by varying the thermal expansion coefficient difference between constituent beams and geometrical arrangements. Our experimental results match qualitatively with a simple scaling law and quantitatively with computational models.

DOI: [10.1103/PhysRevLett.117.175901](https://doi.org/10.1103/PhysRevLett.117.175901)

Solid materials usually expand when heated because the rising temperature induces the elongation of interatomic bonds that manifests itself as volume expansion at the macroscale. However, a number of exceptional solids contract with raising temperatures, exhibiting negative thermal expansions (NTEs) [1–3]. These solids are especially useful for applications where the mismatch in thermal stress should be carefully managed, such as microchip devices [4], adhesive fillers, dental filling [5], and high precision optical or mechanical devices [4,6] under environmental conditions with variable temperatures. The NTE effects of these bulk solids are usually attributed to the thermal-induced geometric rotations of molecular units that lead to effective volume shrinkage [1–3]. And the molecular unit rotations can usually be achieved by atomic interaction or phase transformation within the flexible molecular structures [1–3].

Inspired from the molecular mechanisms of the NTE bulk solids, NTE structures with flexible micro- or macroarchitectures of periodic lattice units have been designed by integrating constituents with varied thermal expansion coefficients (TECs) within single structures. Structural interactions between these constituents with distinct thermal expansion coefficients trigger parts of the structure to rotate or bend to accommodate their thermal expansion within the internal free space, rather than the external space, inducing global volume contraction. Based on this principle, a number of theoretical designs for NTE structures have been proposed to achieve these effects [7–12]. However, the existing experimental validation of NTE effects by using micro-architected structures has been limited to structures with two-dimensional layouts [13–19], while the experimental

realization of three-dimensional negative expansion remains elusive [13,15]. This is primarily due to the difficulty in fabricating three-dimensional composite lattices with multiple material constituents and highly sophisticated geometric connections. In addition, existing NTE structures are built with only limited material choices so that the NTE cannot be well tuned over a large range of temperatures [13–19].

Here, we demonstrate a method to experimentally fabricate three-dimensional composite lattices with tunable NTEs in all three Cartesian directions. The composite lattice is fabricated with a multimaterial projection stereolithography system that enables joining two distinct beam constituents within one lattice structure. The effective volume contraction is induced by constrained thermal expansion of two types of material constituents with different TECs, thus leading to designed deformation. The NTE can be tuned over a large range of temperature by controlling the TECs of the constituent materials and the three-dimensional geometric layout of the structure. The designed mechanism can not only be experimentally implemented in unit cells, but also scaled up by layering the unit cells into large volume three-dimensional lattices. The experimentally observed NTEs are consistent with our scaling theory and numerical simulations.

The fabrication of the NTE structures is realized with a photopolymerization-based multimaterial stereolithography system [Fig. 1(a)] [20–22] that extends the capability of previous single-material stereolithography systems [23–29]. Briefly, we use patterned UV or blue light to cure photocurable presolutions and manufacture three-dimensional structures layer by layer. We switch different presolutions alternatively to enable the manufacturing of multimaterials

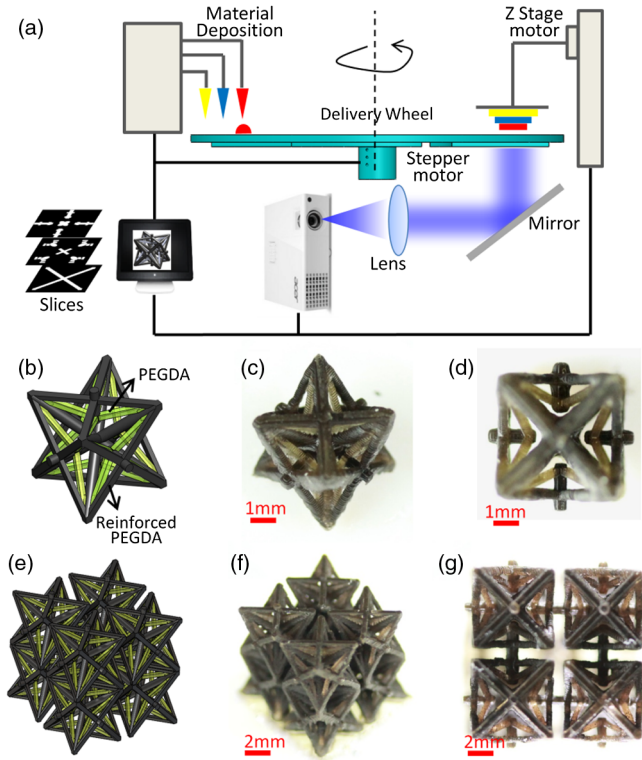


FIG. 1. (a) Schematic of the multimaterial projection microstereolithography system. [(b) and (e)] Computer-aided designs and fabricated samples in [(c) and (f)] three-dimensional and [(d) and (g)] two-dimensional views of the fabricated unit cell and 2 by 2 lattice, respectively.

within a single structure (Fig. S1, Supplemental Material [30]). We employ photocurable poly(ethylene glycol) diacrylate (PEGDA) solutions (molar mass 700, Sigma-Aldrich) doped with varied volume concentrations of copper nanoparticles (50–80 nm, US Research Nanomaterials) as the presolutions. The thermal expansion coefficient of solidified PEGDA is approximately $\alpha_1 = 1.56 \times 10^{-4} \text{ K}^{-1}$. Because of the low TEC ($\sim 2 \times 10^{-5} \text{ K}^{-1}$) and high bulk modulus ($\sim 100 \text{ GPa}$) of the copper particles, the reinforcement with copper particles within PEGDA solids can significantly knock down the TEC (Table S1, Supplemental Material [30], Fig. S2). For example, the TEC of PEGDA solids reinforced with 5% volume of copper nanoparticles becomes $\alpha_2 = 5.1 \times 10^{-5} \text{ K}^{-1}$, around one third of PEGDA's TEC. The larger the volume concentration of copper reinforcement, the lower the resulting TEC (Table S1, Supplemental Material [30], Fig. S2). It is noted that the high volume concentration of copper significantly elongates the printing time of each layer and also decreases the bonding force between printed layers. We are able to print PEGDA beams with up to 10% volume copper within a reasonable time scale (~ 6 hours for each structure).

We design three-dimensional composite structures in the form of cubic unit cells as shown in Figs. 1(b)–1(d). The unit cell [Fig. 1(b)] is composed of a copper-reinforced

PEGDA beam frame (black, $\alpha_2 = 4\text{--}6.1 \times 10^{-5} \text{ K}^{-1}$) and internal tilted PEGDA beams (green). When heated, the PEGDA beams expand more than the copper-reinforced PEGDA beams, thus causing the reinforced beams around the cubic surfaces to bend inward occupying the internal open spaces. Therefore, the overall occupied volume of the structure becomes smaller exhibiting so-called NTE. In the fabricated structure [Fig. 1(c)], the pale yellow PEGDA beams and gray reinforced beams form freely standing unit cell structures with size around 6 mm and beam thickness around 200–500 μm . The additive manufacturing is performed by stacking ~ 200 layers (each material being 100 layers) with each layer being $\sim 60 \mu\text{m}$.

The thermal expansion properties of the fabricated composite structures are measured within a glass thermal chamber ($5 \times 5 \times 2 \text{ cm}$) with a controlled temperature measured by a thermometer (variation $\pm 10 \text{ K}$ within the chamber) (Fig. S3). We gradually increase the temperature from room temperature and wait 30 min for each step to ensure a stable temperature distribution. We then observe the structure deformation with a camera mounted on the top of the glass chamber. It is noted that the observation can only capture deformations in two planar directions; however, we can flip the structure to observe the thermal-induced deformation in the other direction.

As the temperature in the chamber is gradually increased, the composite structure first maintains the size during the initial temperature segment (e.g., 300–350 K), and then bends inward to decrease its size monotonically as a temperature of $\sim 521 \text{ K}$ is approached [Fig. 2(a) and supplemental movie S1]. We keep the temperature below 530 K because the properties of the material constituents will significantly degrade above 550 K. To quantify the results, we define the effective thermal expansion ratio η as the lateral expansion ratio [Fig. 2(a)], namely, $\eta = (L - L_0)/L_0$, where L_0 and L are the lateral size of the unit cell at the initial and heated states, respectively. We then plot the effective expansion ratio as a function of the temperature in Figs. 2(c) and 2(d). The error bar in the effective expansion ratio η comes from the standard deviation along the three primary Cartesian directions of the unit cells. The thermally induced nonlinear geometrical deformation can be understood within three thermal segments via following logic.

We examine the simplest element of the designed structure shown in Fig. 3(a). In the initial thermal segment (298–350 K), to accommodate the thermal expansion, node *B* may follow two different bifurcation paths [Fig. 3(b)]: inward (path 1) or outward (path 2). Instinctively, node *B* is expected to move inward by following path 1 [Fig. 3(bi, ii–iii)], because with increasing temperature beams *AC* and *CF* with larger thermal expansion coefficient expand significantly to pull beams *BC* and *BE* inward (tap *BE* is used to connect the other unit within the lattice). However, from the experimental observation, node *B* first moves outward a little and then snaps inward by

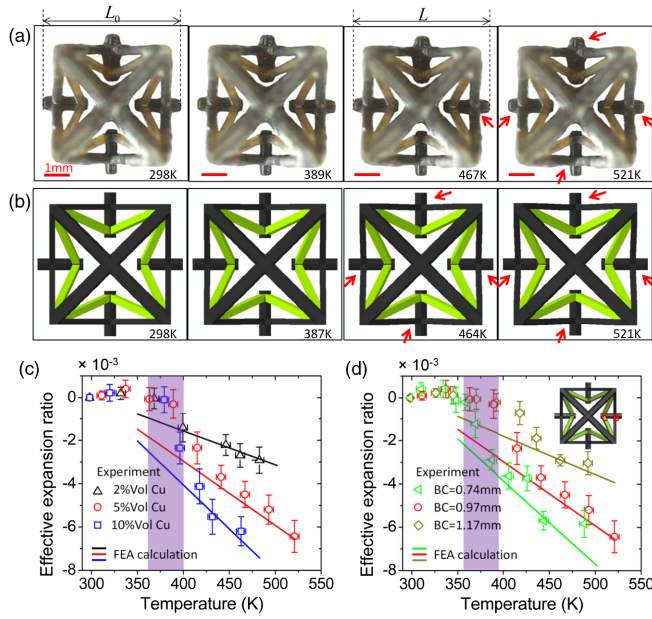


FIG. 2. (a) Experimental and (d) finite element simulation sequences of a unit cell with increasing temperature. The red arrows indicate the inward bending of the reinforced PEGDA beams. [(c)–(d)] Experimentally observed and computationally calculated effective expansion ratios varied with increasing temperatures, (c) with varied volume concentrations of reinforced copper nanoparticles and (d) with varied lengths of beam BC [indicated in the inset of (d)]. The shadow areas in (c) and (d) show the snap-through temperature range. The FEA-simulated negative-thermal-expansion coefficients are -1.57×10^{-5} , 2.91×10^{-5} , and $-4.06 \times 10^{-5} \text{ K}^{-1}$ in (c), and -1.71×10^{-5} , 2.91×10^{-5} , and $-3.93 \times 10^{-5} \text{ K}^{-1}$ in (d), respectively.

following path 2 [Fig. 3(bi, iv–vi)]. The behavior from Fig. 3(bi) to Fig. 3(iv) is because thermal transport within the copper-reinforced PEGDA beams (AB , CE , and BF) is much faster than that within the pure PEGDA beams (AC and CF), and the reinforced beams thermally expand more in the very beginning of the temperature increase. Under this circumstance, beams AC and CF become obstacles to prevent node B from moving inward; therefore, node B can only move outward [Fig. 3(bi–biv)]. However, node B only moves outward slightly with a very small angle ψ [Fig. 3(biv)] and is then trapped at the position, because once beams AC and CF are fully thermal expanded, beam BC is pulled inward and locked.

With increasing temperature (350–400 K), node B is expected to snap through from outside the structure [Fig. 3(biv)] to inside the structure [Fig. 3(bv)]. To trigger this snap-through transition, the system needs to overcome an energy barrier because beams AB and BF should first become shorter and then longer. Only under a perturbation with a significant amplitude can this snap-through transition occur [31]. One possible perturbation can be the thermal-induced buckling of beams AB and BF . Since $\psi \sim 0$, the thermal-induced force within beam AB can be

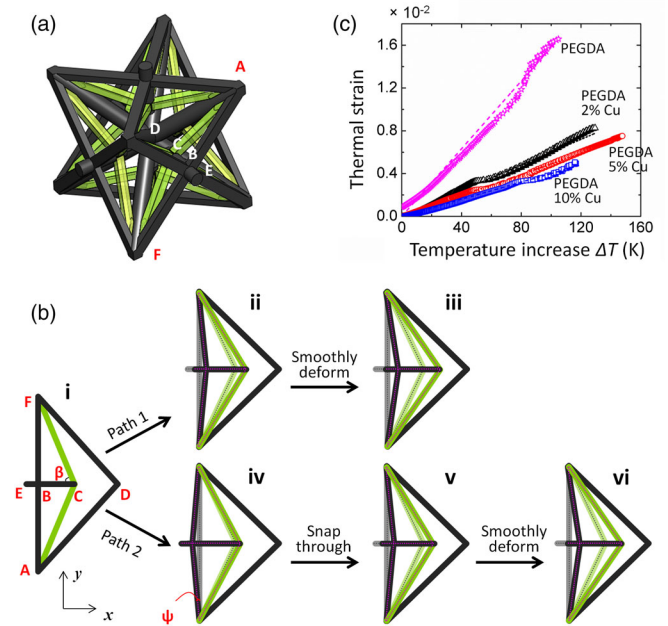


FIG. 3. (a) A unit cell model to illustrate the key nodes. (b) Two bifurcation deformation paths of the simplest model with key nodes illustrated in (a). In path 1, node B moves inward with increasing temperature. In path 2, node B first moves outward, then snaps through inward, and smoothly moves inward with increasing temperature. (c) The thermal-induced strain in reinforced PEGDA beams with various copper reinforcement fractions in functions of temperature increase.

approximated as $\sim \alpha_2 \Delta T E_{AB} A_{AB}$, where ΔT is the temperature increase, α_2 is the thermal expansion coefficient of the reinforced beam, and E_{AB} and A_{AB} are the Young's modulus and cross section area of beam AB , respectively. The critical compressive force for the buckling of beam AB is $\pi^2 E_{AB} I_{AB} / (4L_{AB}^2)$, where the second moment of area $I_{AB} = b_{AB} h_{AB}^3 / 12$, and b_{AB} and h_{AB} are the width and thickness of beam AB , respectively [32]. By equating these two forces, we obtain the critical temperature increase for the buckling of beam AB (of BF), namely, the snap-through transition shown in Fig. 3(biv–bv), as

$$\Delta T_c \sim \frac{\pi^2}{3\alpha_2} \left(\frac{h_{AB}}{L_{AB}} \right)^2. \quad (1)$$

By inputting $h_{AB} \sim 300 \mu\text{m}$, $L_{AB} \sim 4.24 \text{ mm}$, and $\alpha_2 \sim 4\text{--}6.1 \times 10^{-5} \text{ K}^{-1}$, we estimate the critical temperature increase for the snap through as 68.5–102.8 K. The theoretical estimation is roughly consistent with the experimental observation [55–100 K in shadow areas in Figs. 2(c) and 2(d)].

With further increasing temperature [above 400 K, Fig. 3(bv–bvi)], beams AC and CF with larger TEC expand significantly to smoothly pull beams BC and BE inward. To understand this problem in the simplest way, we only consider the thermal expansion without elastic stress response and assume node D is fixed due to the symmetry. The displacement of node C induced by thermal expansion

of beam AC is $\sim \alpha_1 \Delta T L_{AC} / \cos \beta$, where α_1 is the thermal expansion coefficient of the PEGDA beam, L_{AC} is the length of beam AC , and β is the angle between beam AC and beam BC . The displacement of node A in x direction induced by the thermal expansion of beam AD is $\sim -\alpha_2 \Delta T L_{AD} / \sqrt{3}$, where L_{AD} is the length of beam AD . The displacement of node E in x direction can thus be approximated as

$$d_E \sim \frac{\alpha_1 \Delta T L_{AC}}{\cos \beta} - \alpha_2 \Delta T \left(L_{BC} + L_{BE} + \frac{L_{AD}}{\sqrt{3}} \right), \quad (2)$$

where L_{BC} and L_{BE} are the length of beam BC and BE , respectively. The effective expansion ratio can be calculated as

$$\eta \sim -\frac{2d_E}{\sqrt{2}L_{AB} + 2L_{BE}} \sim -\sqrt{2}\Delta T \alpha_1 \left(\frac{2}{\sin 2\beta} - \frac{k}{\tan \beta} - \frac{kL_{BE}}{L_{AB}} - \frac{\sqrt{2}}{2} \right) \left(\frac{1}{1 + \frac{\sqrt{2}L_{BE}}{L_{AB}}} \right), \quad (3)$$

where $k = \alpha_2 / \alpha_1$. Equation (3) is a qualitative scaling of the effective expansion ratio and it does not account for the stress response of the constituent beams. More detailed thermoelastic analysis is given in the Supplemental Material [30,33]. Nevertheless, Eq. (3) may be already sufficient to provide enough insight to design composite structures with large negative thermal expansion.

First, the connector tap beam BE should be set as short as possible to achieve large negative thermal expansion. In the experiments we usually set the BE length to be very small (e.g., $\sqrt{2}L_{BE} \ll L_{AB}$) and fixed in the following discussions. Therefore, Eq. (3) can be reduced as

$$\eta \sim -\sqrt{2}\Delta T \alpha_1 \left(\frac{2}{\sin 2\beta} - \frac{k}{\tan \beta} - \frac{\sqrt{2}}{2} \right). \quad (4)$$

Second, to achieve a large value of η , the TEC of beam AC should be as large as possible (α_1 large) and the TEC of the reinforced beams (AB , BC , and AD) should be as small as possible (k small). In the experiments, we keep the TEC of the PEGDA beams (α_1) and vary the TEC of reinforced beams (α_2) by doping different volume concentrations of copper nanoparticles in the PEGDA. By varying the copper volume fraction from 2% to 10%, the TEC of the reinforced beam decreases from 6.1×10^{-5} to $4.0 \times 10^{-5} \text{ K}^{-1}$ [Fig. 3(c), Table S1], and the effective expansion ratio of the composite unit cell increases accordingly [fabricated unit cells in Fig. S4 and data in Fig. 2(c)]. It is noted that it is not necessary for the higher reinforced concentration to lead to higher effective expansion ratios because the higher reinforced concentration also induces higher rigidity (Table S1), which makes the reinforced beams more difficult to deform.

Third, from Eq. (4), the effective negative-thermal-expansion ratio increases with increasing angle β (Fig. S5).

If we fix the length of beam AB , the angle β is controlled by the length of beam BC . Therefore, we fabricate composite structures with varied beam BC length (Fig. S6) and confirm that the negative thermal expansion indeed increases by decreasing BC length from 1.17 to 0.74 mm [Fig. 2(d)]. It is noted that when β is approaching its limits of $\pi/2$ or $\text{atan}(\sqrt{2})$, the interaction between the PEGDA beam AC and reinforced beams AB and AD may have a large volume of overlaps; therefore, around these two limiting values, the effective expansion ratio does not necessarily increase with the angle β .

To further quantitatively understand the structure and validate the experimental results, we perform finite element analyses (FEA) with measured mechanical properties [Table S1 and Figs. 3(c) and S8]. Since the composite structures are fabricated additively layer by layer (Fig. S7), we measure the Young's modulus and thermal expansion coefficient in two orthogonal directions. However, the measured results in two directions differ slightly (Table S1 and Fig. S8). Therefore, we treat the beams in our FEA models as homogeneous linear thermoelastic solids with the effective properties in Table S1. By considering the symmetry of the problem, we only analyze 1/8 of the unit cell [Fig. S9(a)] and model it as a three-dimensional thermomechanical problem [two-dimensional view in Fig. 2(b), supplemental movie S2, three-dimensional view in Fig. S9(b), and supplemental movie S3]. Overall, our FEA results approximately agree with the experimental results (Fig. 2).

The unit cell design of negative-thermal-expansion composites can be scaled up to a larger volume lattice. The composite lattices are formed by connecting the middle tabs of unit cells [Fig. 4(a)]. When heated, the middle tabs

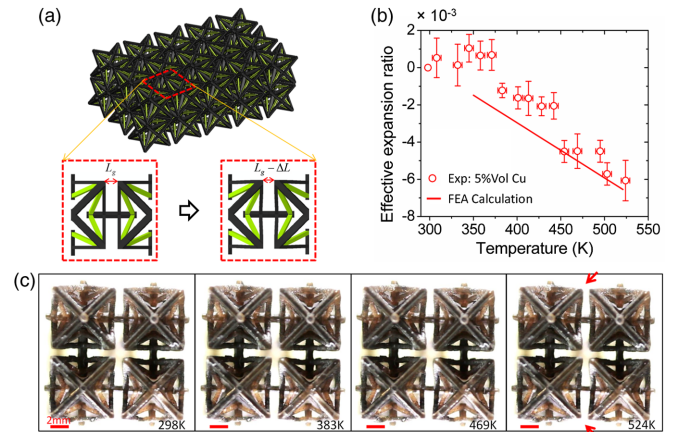


FIG. 4. (a) A CAD model of a composite lattice by layering a number of unit cells. The inset of (a) shows the deformation mechanism between unit cells within the composite lattice. (b) Experimentally observed and computationally calculated effective expansion ratios and (c) experimental sequences of a 2 by 2 composite lattice under raising temperature. The arrows indicate the deformation.

move towards the internal free space of the unit cells, and the corners of two unit cells thus squeeze the gap between the unit cells [Fig. 4(a)]. For example, when heated the gap distance may reduce from L_g to $L_g - \Delta L$. Therefore, the overall occupied volume of the lattice decreases with the increasing temperature. To demonstrate the concept, we fabricated 2 by 2 by 2 lattices with PEGDA beams and reinforced beams with 5% volume copper [Figs. 1(e)–1(g)]. The lattice indeed exhibits large NTE ($\sim -2.9 \times 10^{-5} \text{ K}^{-1}$) over a large range of temperature (350–524 K) [Figs. 4(b) and 4(c) and supplemental movie S4]. The NTE coefficient is very close to that of the corresponding unit cells [$\sim -2.96 \times 10^{-5} \text{ K}^{-1}$ in Figs. 2(c) and 2(d)], confirming that layering unit cells into a large volume lattice does not compromise the overall NTE performance. In addition, the experimental results also agree with the finite element analysis [Fig. 4(b)].

As shown in Figs. 2(c) and 2(d) and 4(b), the effective negative thermal expansion of the unit cell can be tuned over a factor of 3, from -1.57×10^{-5} to $-4.06 \times 10^{-5} \text{ K}^{-1}$ by varying the copper volume concentration from 2% to 10%, and from -1.78×10^{-5} to $-3.85 \times 10^{-5} \text{ K}^{-1}$ by varying the length of beam BC . The negative thermal expansion is in a reasonable range compared with the existing theoretical studies and experimental demonstrations of NTE lattices [7–19]. To the best of our knowledge, the current work is the first experimental demonstration that shows large tunability of negative thermal expansion in three dimensions in microlattice structures. In addition, the negative thermal expansion which exhibits itself over a large range of temperature, i.e., ~ 350 to ~ 520 K, can enable potential applications within an environment with large temperature variations. Moreover, the fabricated lattice [Fig. 1(f)] is highly porous and lightweight with ultralow density ($\sim 0.23 \text{ g/cm}^3$), much smaller than the densities of the PEGDA solid (1.13 g/cm^3) and copper-reinforced PEGDA solid (5% volume, 1.52 g/cm^3).

In summary, we fabricated three-dimensional multimaterial composite lattices consisting of solid beams with distinct TECs resulting in tunable negative thermal expansion. We developed a simple scaling law to qualitatively understand the beam-interaction induced negative thermal expansion. Guided by the scaling law, the NTE of composite unit cells can be tuned by varying the TEC differences and geometrical arrangements. We also demonstrate that the unit cells can be tessellated into large volume lattices with significant NTEs. We expect our designs of three-dimensional NTE lattices and experimental fabrication can contribute to a number of potential applications where thermal stress should be carefully managed and materials with minimum or negative thermal expansion can mitigate the thermal damage or improve instrument accuracy over large temperature variations. Specifically, zero-thermal-expansion structures may be realized with our additive manufacturing system, through

judiciously offsetting the positive and negative effects within the lattices, or assembling NTE structures with positive-thermal-expansion solids in interdigitated patterns. The low dielectric constant of such composite material would also offer promising applications for printed circuit boards with low losses that can survive high temperature differences. In addition, used thermoplastic PEGDA does not show optimal thermal cyclability and manufacturing with materials with better thermal cyclability can significantly improve the structural durability.

We acknowledge the financial support of the DARPA Materials with Controlled Microstructural Architectures program (Program Manager Dr. Judah Goldwasser). Portions of this work were conducted under the auspices of the U.S. Department of Energy by Lawrence Livermore National Laboratory under Award No. DE-AC52-07NA27344 (LLNL-JRNL-697779). Q.W. thanks the startup fund from the University of Southern California and NSF Grant No. 1649093. N.X.F. acknowledges the financial support by the Office of Naval Research, Multidisciplinary University Research Initiative (Grant No. N00014-13-1-0631). Q.G. acknowledges support from the SUTD-MIT joint postdoctoral program.

*qimingw@usc.edu

†nicfang@mit.edu

- [1] K. Takenaka, *Sci. Technol. Adv. Mater.* **13**, 013001 (2012).
- [2] G. D. Barrera, J. A. O. Bruno, T. H. K. Barron, and N. L. Allan, *J. Phys. Condens. Matter* **17**, R217 (2005).
- [3] W. Miller, C. Smith, D. Mackenzie, and K. Evans, *J. Mater. Sci.* **44**, 5441 (2009).
- [4] C. Closmann, A. Sleight, and J. Haygarth, *J. Solid State Chem.* **139**, 424 (1998).
- [5] A. Versluis, W. H. Douglas, and R. L. Sakaguchi, *Dental materials* **12**, 290 (1996).
- [6] W. J. Clegg and A. Kelly, *Adv. Eng. Mater.* **4**, 388 (2002).
- [7] O. Sigmund and S. Torquato, *Appl. Phys. Lett.* **69**, 3203 (1996).
- [8] R. Lakes, *Appl. Phys. Lett.* **90**, 221905 (2007).
- [9] M. Hirota and Y. Kanno, *Optim. Eng.* **16**, 767 (2015).
- [10] J. Lehman and R. Lakes, *J. Intell. Mater. Syst. Struct.* **23**, 1263 (2012).
- [11] J. Lehman and R. Lakes, *J. Mater. Res.* **28**, 2499 (2013).
- [12] J. B. Hopkins, H. Lee, N. X. Fang, and C. M. Spadaccini, in *ASME 2015 International Design Engineering Technical Conferences and Computers and Information in Engineering Conference* (American Society of Mechanical Engineers, Boston, 2015), p. V02BT03A006.
- [13] A. Takezawa, M. Kobashi, and M. Kitamura, *APL Mater.* **3**, 076103 (2015).
- [14] J. Qi and J. W. Halloran, *J. Mater. Sci.* **39**, 4113 (2004).
- [15] C. A. Steeves, S. L. dos Santos e Lucato, M. He, E. Antinucci, J. W. Hutchinson, and A. G. Evans, *J. Mech. Phys. Solids* **55**, 1803 (2007).
- [16] J. Berger, C. Mercer, R. M. McMeeking, and A. G. Evans, *J. Am. Ceram. Soc.* **94**, s42 (2011).

- [17] E. Gdoutos, A. Shapiro, and C. Daraio, *Exp. Mech.* **53**, 1735 (2013).
- [18] C. A. Steeves, C. Mercer, E. Antinucci, M. Y. He, and A. G. Evans, *Int. J. Mech. Mat. Des.* **5**, 195 (2009).
- [19] N. Yamamoto, E. Gdoutos, R. Toda, V. White, H. Manohara, and C. Daraio, *Adv. Mater.* **26**, 3076 (2014).
- [20] K. Arcaute, B. Mann, and R. Wicker, *Acta Biomater.* **6**, 1047 (2010).
- [21] J.-W. Choi, H.-C. Kim, and R. Wicker, *J. Mater. Process. Technol.* **211**, 318 (2011).
- [22] C. Zhou, Y. Chen, Z. Yang, and B. Khoshnevis, *Rapid Prototyping J.* **19**, 153 (2013).
- [23] X. Zheng, J. Deotte, M. P. Alonso, G. R. Farquar, T. H. Weisgraber, S. Gemberling, H. Lee, N. Fang, and C. M. Spadaccini, *Rev. Sci. Instrum.* **83**, 125001 (2012).
- [24] X. Zheng *et al.*, *Science* **344**, 1373 (2014).
- [25] H. Lee, J. Zhang, H. Jiang, and N. X. Fang, *Phys. Rev. Lett.* **108**, 214304 (2012).
- [26] J. Bauer, S. Hengsbach, I. Tesari, R. Schwaiger, and O. Kraft, *Proc. Natl. Acad. Sci. U.S.A.* **111**, 2453 (2014).
- [27] L. R. Meza, S. Das, and J. R. Greer, *Science* **345**, 1322 (2014).
- [28] J. R. Tumbleston *et al.*, *Science* **347**, 1349 (2015).
- [29] T. A. Schaedler, A. J. Jacobsen, A. Torrents, A. E. Sorensen, J. Lian, J. R. Greer, L. Valdevit, and W. B. Carter, *Science* **334**, 962 (2011).
- [30] See Supplemental Material at <http://link.aps.org/supplemental/10.1103/PhysRevLett.117.175901> for Supplemental methods, figures and movies.
- [31] J. M. T. Thompson and G. W. Hunt, *Elastic Instability Phenomena* (Wiley Chichester, New York, 1984).
- [32] S. P. Timoshenko and J. M. Gere, *Theory of Elastic Stability* (Courier Corporation, North Chelmsford, 2009).
- [33] J. D. Renton, *Elastic Beams and Frames* (Elsevier, New York, 2002).